

# A Bayesian framework for active object recognition, pose estimation and shape transfer learning through touch

Haodong Zheng, Andrei Jalba, Raymond H. Cuijpers, Wijnand IJsselsteijn, Sanne Schoenmakers

**Abstract**—As humans can explore and understand the world through the sense of touch, tactile sensing is also an important aspect of robotic perception. In unstructured environments, robots can encounter both known and novel objects, this calls for a method to address both known and novel objects. In this study, we combine a particle filter (PF) and Gaussian process implicit surface (GPIS) in a unified Bayesian framework. The framework can differentiate between known and novel objects, perform object recognition, estimate pose for known objects, and reconstruct shapes for unknown objects, in an active learning fashion. By grounding the selection of the GPIS prior with the maximum-likelihood-estimation (MLE) shape from the PF, the knowledge about known objects’ shapes can be transferred to learn novel shapes. An exploration procedure with global shape estimation is proposed to guide active data acquisition and conclude the exploration when sufficient information is obtained. The performance of the proposed Bayesian framework is evaluated through simulations on known and novel objects, initialized with random poses. The results show that the proposed exploration procedure, utilizing global shape estimation, achieves faster exploration than a local exploration procedure based on rapidly explore random tree (RRT). Overall, our results indicate that the proposed framework is effective and efficient in object recognition, pose estimation and shape reconstruction. Moreover, we show that a learned shape can be included as a new prior and used effectively for future object recognition and pose estimation.

**Index Terms**—Bayesian inference, robotics, tactile perception, active learning, object recognition, pose estimation, shape reconstruction

## I. INTRODUCTION

Tactile sensing is an important aspect of robot sensing, and it is useful both to complement vision, but also as a standalone sensing modality. Visual information is not always available and reliable, especially under severe occlusions and poor lighting conditions. Therefore, methods that can work regardless of the visual information availability are desired, to have robots function well in natural or unstructured environments. In this study, we focus on localizing and recognizing objects based on the shape of the object, solely through touch. Knowing the object’s shape and pose is important for locating and manipulating objects, and therefore, it is useful for a variety of applications.

In unstructured environments, both known and novel objects can be encountered, nonetheless, how to address both known and novel objects under an unified framework remains

This study is funded by the Eindhoven Artificial Intelligence Systems Institute. All authors are affiliated with Eindhoven University of Technology.

an open question. Identifying known and unknown objects, and addressing them accordingly is therefore of paramount importance. For known objects, the object class and pose should be estimated, whereas, for a novel object, its shape should be explored and learned. Previous work tends to separate the processes of object recognition, pose estimation, and shape reconstruction. In this study, we combine these goals. Moreover, we explore the possibility of transferring knowledge from known object shapes to learn novel shapes by addressing these novel objects within the same framework that has obtained prior knowledge about objects.

Compared to robotic vision, robotic tactile sensors provide sparse data that are often insufficient for resolving uncertainty in the object class/shape and pose estimation. Especially when the tactile sensors are small compared to the size of the object in contact, only local information is available. Therefore, tactile exploration needs to be performed in an active manner to reduce the uncertainty in object class, pose and shape.

With the recent advancement of tactile sensing technology, vision-based tactile sensors [1], [2] have gained popularity, as they provide accurate and detailed information on the local geometry of the contact area, although they are still less accessible due to their relatively high cost and complicated manufacturing procedure. In this study, we assume the input to the system to be a contact mask with the sensor location and a surface normal vector when in contact. The sensor’s location and orientation can be extracted from robot’s proprioception through forward kinematics, while the normal vector can be estimated based on the sensor’s orientation.

A Bayesian-based approach is a good choice for the problem introduced in this study, because it allows for straightforward integration of prior knowledge with sensor data, and it has an explicit uncertainty treatment. Therefore, we use a Bayesian framework to jointly estimate the object class and object pose with active exploration from first contact to conclusion. Moreover, the proposed framework can identify and learn the shape of novel objects through Bayesian evidence tracking and transfer learning.

An outline of the proposed framework is shown in Fig. 1. The particle filter (PF) is in charge of online updating the joint distribution of object class and pose, while more data are collected. Taking inspiration from the Manifold particle filter [3] and point-pair features proposed in [4], we modify a traditional particle filter [5] to progressively sample new particles based on newly observed data points. Therefore, our particle filter can deal with arbitrary initial uncertainty. In addition, this

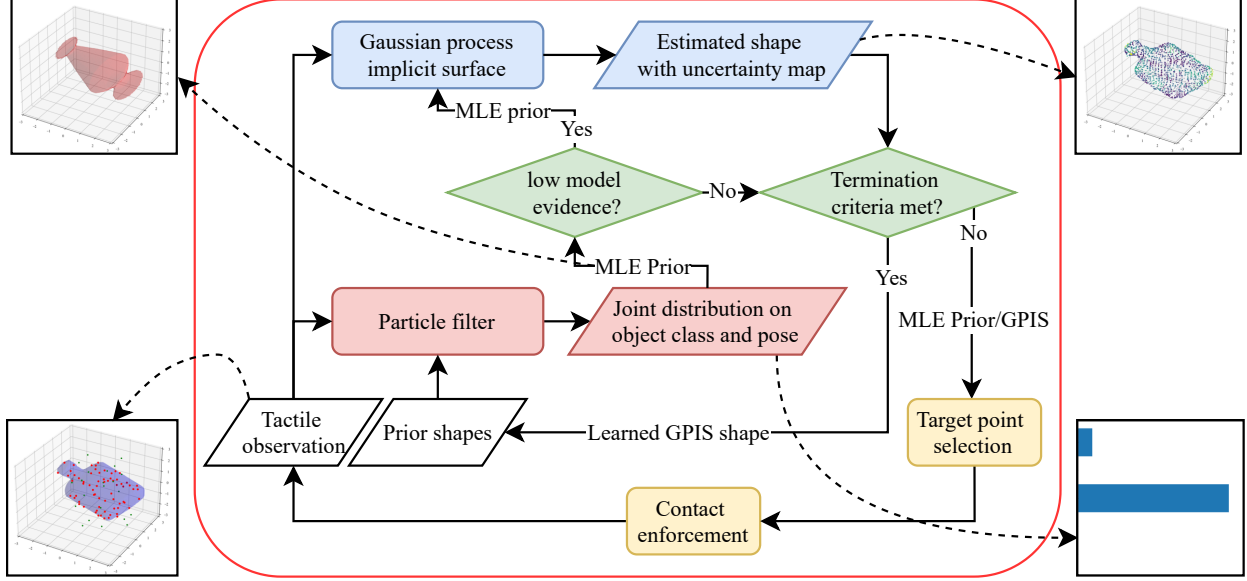


Fig. 1. The proposed framework consists of a particle filter (PF) and a Gaussian process implicit surface (GPIS). The maximum likelihood estimation (MLE) for object class and pose from the PF are used as priors for GPIS reconstruction when a novel object is identified. An exploration procedure, including target point selection and contact enforcement, is proposed to perform active data acquisition.

approach keeps the computational cost tractable at each time step and can achieve low pose estimation error as more data are collected despite using coarse discretized approximation in the PF. The Bayesian evidence of the maximum likelihood estimation (MLE) obtained from the PF is used to determine if the object is a known or novel object. Once a novel object is detected, the MLE from the PF is used as a prior for Gaussian process implicit surface (GPIS) reconstruction. The target point selection and contact enforcement modules take care of the active data acquisition using information from global shape estimation from either the PF or GPIS. A termination criterion is used, based on the Directed Hausdorff Distance (DHD), to determine when the object has been sufficiently explored and a conclusion can be drawn.

The main contributions of this paper are as follows:

- A Bayesian framework is proposed to perform simultaneous object recognition and pose estimation for known objects. In case of novel objects shape transfer learning is applied in an active setting to learn the new shapes.
- The proposed Bayesian framework can capitalize on the knowledge of a learned novel object shape for faster object recognition and pose estimation when the object is later encountered.

## II. RELATED WORK

Our work is closely related to Bayesian-based object recognition, pose estimation, shape reconstruction, and active tactile exploration.

### A. Bayesian Touch-Only Object Recognition and Pose Estimation

Previous work approached the object recognition problem based on material properties. Kaboli et al. and Xu et al.

[6]–[8] used properties such as stiffness, texture, and thermal conductivity to distinguish between different objects. Our method instead focuses on object recognition with geometric information, which can be obtained through most tactile sensors.

Some researchers used methods more in line with our work with touch-based pose estimation of objects. For instance, particle filters (PF) can be used to approximate arbitrary distributions, which makes them suited for capturing the uncertainty of the object pose presented during tactile exploration. However, using a PF comes with a computational challenge as a substantial amount of particles is required to cover the state space. Koval et al. [3] proposed the manifold particle filter by adaptively sampling particles that reside on the contact manifold to increase sampling efficiency. Petrovskaya et al. [9] proposed the Scaling Series algorithm, combining the Bayesian Monte Carlo technique coupled with annealing, to refine the posterior distribution of the 6-degree-of-freedom (DOF) pose through multiple stages with a small number of particles at each stage. Vezzani et al. [10] proposed to use a memory unscented Kalman filter (MUKF) to cover the 6-DOF pose space with a small number of particles where each particle is treated as a Gaussian distribution instead of a discrete sample. Although the methods are quite efficient, the work by [3], [9], [10] was confined to pose estimation. As they limited their scope to the pose estimation of a known object, multi-class classification was not addressed in their work. Vezzani et al. [11] extended their own work on pose estimation [10] to also address object recognition by applying the localization scheme to multiple object classes and picking the object class with the smallest error in localization.

Differing from the aforementioned methods, our proposed framework estimates the joint distribution of object class and object pose by progressively sampling new particles based on newly observed point pairs. The motivation behind this design choice is to avoid tracking all possibilities from the beginning of the exploration. Instead of using all data, the particle filter samples new particles that fit a new point pair generated from the new contact point and a previous observed contact point. Due to the discretized nature of the PF, there is no guarantee that a small number of initial particles can cover the region near the ground truth. By sampling new particles at each time step, the PF can consider more particles throughout active tactile exploration while keeping the number of particles small at each time step through resampling. More importantly, we combine the PF and GPIS to distinguish between known and novel objects and transfer knowledge on known object shapes to learn novel object shapes. Another distinction is that our proposed framework uses an active exploration procedure utilizing the global estimated shape at each time step for active data acquisition.

### B. Bayesian Touch-Only Shape Reconstruction

Gaussian processes (GPs) are widely used for the task of shape reconstruction as they provide uncertainty measurement of the reconstructed surface, which enables Bayesian optimization for selecting actions during exploration. Sun et al. and Jamali et al. [12], [13] used the Gaussian process explicit surface for shape reconstruction, but the choice of representation cannot represent arbitrary shapes. Gaussian process implicit surface (GPIS) [14] was introduced to address this limitation. Several researchers, e.g. [15]–[20], adopted GPIS for active shape reconstruction based on touch. These methods used the same prior for all test objects, which did not explore the possibility of shape transfer learning. Martens et al. [21] proposed to fit a parametric ellipsoid according to the observed point cloud as prior for GPIS reconstruction, whereas our approach updates the maximum likelihood prior continuously to take on the shape of objects in the prior at each time step based on new observations.

### C. Active Tactile Sensing

Due to the local nature of tactile data, robots often need to acquire data actively to obtain sufficient information for object recognition and shape reconstruction. Therefore, good strategies are necessary to perform active exploration efficiently.

1) *Active Exploration Strategies for Object Recognition:* Active learning procedures have been proposed for efficient object recognition by selecting the action with the least expected entropy at the next time step [22]. Other researchers suggested selecting actions that minimize their proposed expected confusion metrics [6]–[8]. In this study, we instead aim to increase data coverage on the estimated object surface and get global context, which leads to the proposed directed Hausdorff distance (DHD) based target point selection procedure.

2) *Active Exploration Strategies for Shape Reconstruction:* Several studies used GP-based approaches. Jamali et al. [13] and Yi et al. [23] proposed active learning procedures that select the next point of interest to be the point with the most uncertainty. Yang et al. [24] proposed a greedy target point selection procedure based on mutual information of the GPIS. Using graph-based planning, Matsubara et al. [25] took into account both surface uncertainty and travel cost to improve the efficiency of tactile exploration. Instead of considering the uncertainty of each point, Driess et al. [18] proposed to generate smooth trajectories with the most uncertainty on the object’s surface for more human-like tactile exploration. Their subsequent study [19] introduced a new loss function based on the differential entropy of the GP to enable multi-finger exploration simultaneously. One problem with GP-based continuous path exploration is that it requires many points to get the global context of the object. In our study, motivated by obtaining global context as soon as possible, the most uncertain point on the GPIS will be selected as the target point when a novel object is detected.

For both known and novel objects, a contact enforcement procedure is performed to attempt to establish contact from the point of interest on the estimated shape. It will resort to local exploration if it fails to establish contact based on the estimated shape.

### D. Deep-Learning-Based Approaches for shape reconstruction

Deep learning methods were developed to address active shape reconstructions. Comi et al. [26] learned a compact vector representation from large object datasets, and created a DeepSDF network conditioned on the learned representation. Based on contact patches from a vision-based tactile sensor, they retrieved the reconstructed shape by finding the shape embedding that yields the most consistent results with the contact. Their work does not consider an active learning setup. Wang et al. [27] and Rustler et al. [28] developed methods to perform active shape completion based on touch data, but their methods relied on information from RGB/RGB-D camera for initialization. Smith et al. [29], [30] proposed graph-neural-network-based methods (GNNs) to reconstruct 3D shapes using vision and touch. Though aiming at visuo-tactile information integration, their methods also work under touch-only settings. In addition, Smith et al. [30] used reinforcement learning to train an active exploration policy for efficient shape reconstruction. However, in contrast to our work, they used a fixed spherical prior for shape reconstruction. The aforementioned methods did not provide the joint distribution of the object class and object pose nor addressed the uncertainty throughout tactile exploration explicitly. In addition, they require a significant amount of training data.

## III. METHODS

In this section, we start by deriving the Bayesian formulation of the object recognition and pose estimation problem, then expand the formulation to include shape reconstruction for novel objects.

### A. Problem Formulation

To estimate the object class and object pose through tactile contact points and surface normal vectors at these points, we consider the joint distribution of the object class and object pose, given the tactile observations., since both object class and pose determine whether, or not, contact with the object can be observed at a certain location. Often an object is held stationary by one hand and explored by the other hand, therefore, for simplicity, we assume that the object's pose is stationary during tactile exploration of the robotic arm.

The object class  $c$  and the object pose  $\mathbf{p} \leftarrow [p_x, p_y, p_z, \alpha, \beta, \gamma]$  are concatenated into a latent variable vector  $\mathbf{z}$ , where  $[p_x, p_y, p_z]$  represents the origin coordinates of the object frame in the world frame and  $[\alpha, \beta, \gamma]$  denote the relative yaw, pitch, and roll angles of the object frame in the world frame. Each observed data point coordinate  $[u_x, u_y, u_z]^T$  is denoted as  $\mathbf{x}$ . Likewise, the observed signed distance value  $d_s$  and surface normal vector  $[n_x, n_y, n_z]$  at each data point  $\mathbf{x}$ , is concatenated into a vector  $\mathbf{d}$ , i.e.,

$$\mathbf{z} \leftarrow [c, \mathbf{p}] \quad (1)$$

$$\mathbf{d} \leftarrow [d_s, \mathbf{n}] \quad (2)$$

$$\begin{cases} d_s = 0 & \text{on surface} \\ d_s > 0 & \text{outside object} \\ d_s < 0 & \text{inside object} \end{cases} \quad (3)$$

Given an object class  $c$  and object pose  $\mathbf{p}$ , the predicted Euclidean signed distance value  $\hat{d}_s$  from a point  $\mathbf{x}$  to the object surface is given by its signed distance function

$$\hat{d}_s := f(\mathbf{x}, \mathbf{z}), \quad (4)$$

where  $f$  denotes the Euclidean signed distance function.

The predicted surface normal  $\hat{\mathbf{n}}$  at a contact point  $\mathbf{x}$  could be calculated by differentiation, i.e.,

$$\hat{\mathbf{n}} = \nabla_{\mathbf{x}} f(\mathbf{x}, \mathbf{z}). \quad (5)$$

The predicted value of  $\mathbf{d}$  is denoted as  $\hat{\mathbf{d}}$ , where

$$\hat{\mathbf{d}} \leftarrow [\hat{d}_s, \hat{\mathbf{n}}]. \quad (6)$$

### B. Bayesian Inference for Simultaneous Object Recognition and Pose Estimation and Shape Reconstruction through Touch

Let  $\mathbf{D}$  denote the set of all observed tactile signals  $\mathbf{d}$  and  $\mathbf{X}$  be the set of all locations  $\mathbf{x}$  where  $\mathbf{D}$  are observed. Given tactile sensory data  $\mathbf{D}$  at locations  $\mathbf{X}$ , the aim is to estimate the latent variables  $\mathbf{z}$ . Based on Bayes' theorem, the posterior distribution on  $\mathbf{z}$  can be calculated as follows,

$$p(\mathbf{z}|\mathbf{D}, \mathbf{X}) = \frac{p(\mathbf{D}|\mathbf{z}, \mathbf{X})p(\mathbf{z})}{\sum_{\mathbf{z}} p(\mathbf{D}, \mathbf{z}|\mathbf{X})} \propto p(\mathbf{D}|\mathbf{z}, \mathbf{X})p(\mathbf{z}) \quad (7)$$

where  $p(\mathbf{z})$  is the prior joint distribution of object class and object pose,  $p(\mathbf{D}|\mathbf{z}, \mathbf{X})$  denotes the measurement likelihood function, which represents the likelihood of observing tactile sensory data  $\mathbf{D}$  at locations  $\mathbf{X}$  assuming the object class is  $c$  and the pose is  $\mathbf{p}$ ;  $p(\mathbf{d}|\mathbf{z}, \mathbf{x})$  is the observation likelihood function for a single data point. In this paper,  $p(\mathbf{z})$  is chosen

to be a uninformative uniform distribution  $U$ . For simplicity, in our formulation, each observation  $\mathbf{d}$  at location  $\mathbf{x}$  is assumed to be independent from other observations, given the latent variables  $\mathbf{z}$  is known. This simplifies (7) into,

$$p(\mathbf{D}|\mathbf{z}, \mathbf{X}) = \prod_{i=1}^O p(\mathbf{d}_i|\mathbf{z}, \mathbf{x}_i), \quad (8)$$

where the subscript  $i$  denotes the index of each observed data point, and  $O$  denotes the total number of observed data points.

As the proposed framework actively acquires data, at each time step  $t$ , new tactile data  $\mathbf{D}_t$  are observed at locations  $\mathbf{X}_t$ . Let  $T$  denote the total time steps passed,  $\mathbf{D}_{1:T}$  represent all observed tactile data from time step 1 to  $T$  and  $\mathbf{X}_{1:T}$  denote the locations where  $\mathbf{D}_{1:T}$  are observed; then (7) can be rewritten as

$$p(\mathbf{z}|\mathbf{D}_{1:T}, \mathbf{X}_{1:T}) = \frac{p(\mathbf{z}, \mathbf{D}_{1:T}|\mathbf{X}_{1:T})}{\sum_{\mathbf{z}} p(\mathbf{z}, \mathbf{D}_{1:T}|\mathbf{X}_{1:T})}. \quad (9)$$

As we assume independence between different observations given  $\mathbf{z}$ , the joint distribution can be calculated as

$$\begin{aligned} p(\mathbf{z}, \mathbf{D}_{1:T}|\mathbf{X}_{1:T}) &= p(\mathbf{z})p(\mathbf{D}_{1:T-1}|\mathbf{z}, \mathbf{X}_{1:T-1})p(\mathbf{D}_T|\mathbf{z}, \mathbf{X}_T) \\ &= p(\mathbf{z}, \mathbf{D}_{1:T-1}|\mathbf{X}_{1:T-1})p(\mathbf{D}_T|\mathbf{z}, \mathbf{X}_T). \end{aligned} \quad (10)$$

One can obtain the MLE  $\mathbf{z}^*$  of the object pose and object class given observed data as follows,

$$\mathbf{z}^* := \underset{\mathbf{z}}{\operatorname{argmax}}(p(\mathbf{z}|\mathbf{D}_{1:T}, \mathbf{X}_{1:T})) \quad (11)$$

To decide if the object is known or unknown, one can track the consistency between the  $\mathbf{z}^*$  and the observed data  $\mathbf{D}_{1:T}$  by calculating  $p(\mathbf{D}_{1:T}|\mathbf{z}^*, \mathbf{X}_{1:T})$  using (8). In the following sections,  $p(\mathbf{D}_{1:T}|\mathbf{z}^*, \mathbf{X}_{1:T})$  is referred to as MLE model evidence. A low value for  $p(\mathbf{D}_{1:T}|\mathbf{z}^*, \mathbf{X}_{1:T})$ , when the object surface is fully explored, would imply the test object is unknown.

### C. Measurement Likelihood Function

The measurement likelihood function is defined based on the difference between the predictive signed distance values, normal vectors and the observed values. The observed signed distance value  $d_s$  at a contact location  $\mathbf{x}$  is always regarded as zero.

If we assume that each tactile observation  $\mathbf{d}$  at location  $\mathbf{x}$  follows a Gaussian distribution,

$$\mathbf{d} \sim N(\hat{\mathbf{d}}, \Sigma) \quad (12)$$

$$\Sigma = \operatorname{diag} \left( \left[ \frac{1}{2\sigma_d^2}, \frac{1}{2\sigma_n^2}, \frac{1}{2\sigma_n^2}, \frac{1}{2\sigma_n^2} \right] \right). \quad (13)$$

In other words, the measurement likelihood function satisfies:

$$p(\mathbf{d}|\mathbf{z}, \mathbf{x}) = \frac{1}{Z} \exp \left( \hat{\mathbf{d}} - \mathbf{d} \right)^T \Sigma \left( \hat{\mathbf{d}} - \mathbf{d} \right) \quad (14)$$

$$Z = (2\pi)^2 \sqrt{\det(\Sigma)} \quad (15)$$

$$-\ln p(\mathbf{d}|\mathbf{z}, \mathbf{x}) \propto \left( \hat{\mathbf{d}} - \mathbf{d} \right)^T \Sigma \left( \hat{\mathbf{d}} - \mathbf{d} \right), \quad (16)$$

where  $\text{diag}$  is an operator to form a diagonal matrix from a vector,  $Z$  is the normalization constant,  $\sigma_d$  and  $\sigma_n$  denote the standard deviations for the signed distance function observation and surface normal observation respectively.

#### D. Negative Information Update

Equation (14) assumes the observed data takes on precise values. However, when the tactile sensor is not in contact with the object, it implies that, at the sensor location  $\mathbf{x}$ ,  $d_s \in (0, +\infty)$ , and though the normal vector can still be predicted at  $\mathbf{x}$ , it cannot be observed from tactile sensors as no contact force would be sensed in a real setup.

$$p(\mathbf{d}|\mathbf{z}, \mathbf{x}) = p(d_s > 0|\mathbf{z}, \mathbf{x}) = \int_0^\infty p(d_s|\mathbf{z}, \mathbf{x}) dd_s. \quad (17)$$

For the Gaussian likelihood function, the likelihood reads

$$p(d_s > 0|\mathbf{z}, \mathbf{x}) = \frac{1}{2} \left( 1 - \text{erf} \left( \frac{-f(\mathbf{x}, \mathbf{z})}{\sqrt{2}\sigma_d} \right) \right). \quad (18)$$

where  $\text{erf}$  denotes the Gauss error function. By substituting (17) and (18) into (8) the framework can update its belief when no contact is observed at a location  $\mathbf{x}$ .

#### E. Particle Filter (PF) for Object Recognition and Pose Estimation

A particle filter (PF) [5] is adopted to estimate the joint distribution of the object's class and pose online based on equations (11)-(16). The core idea behind particle filters is to use weighted discrete samples (particles) to approximate the posterior distribution of interest based on importance sampling, i.e.,

$$p(\mathbf{z}|\mathbf{D}_{1:t}, \mathbf{X}_{1:t}) = \sum_{j=1}^N w_{j,t} \delta(\mathbf{z} - \mathbf{z}_{j,t}), \quad (19)$$

where the subscript  $j, t$  denotes the index of a particle in the PF at time step  $t$ , and  $\delta$  denotes the Dirac delta function,  $N$  denotes total number of particles. The unnormalized weight of a particle  $w_{j,t}$  can be calculated as

$$\begin{aligned} w_{j,t} &\propto p(\mathbf{z}_{j,t}|\mathbf{D}_{1:t}, \mathbf{X}_{1:t}) \\ &\propto p(\mathbf{z}_{j,t}, \mathbf{D}_t|\mathbf{D}_{1:t-1}, \mathbf{X}_{1:t}) \\ &= p(\mathbf{z}_{j,t}|\mathbf{D}_{1:t-1}, \mathbf{X}_{1:t-1}) p(\mathbf{D}_t|\mathbf{z}_{j,t}, \mathbf{X}_t) \\ &= \sum_{\mathbf{z}_{j,t-1}} (\bar{w}_{j,t-1} p(\mathbf{z}_{j,t}|\mathbf{z}_{j,t-1}, \mathbf{D}_{1:t-1}, \mathbf{X}_{1:t-1})) \times \\ &\quad p(\mathbf{D}_t|\mathbf{z}_{j,t}, \mathbf{X}_t). \end{aligned} \quad (20)$$

Since we assume the object stays static during the exploration, thus

$$p(\mathbf{z}_{j,t}|\mathbf{z}_{j,t-1}, \mathbf{D}_{1:t-1}, \mathbf{X}_{1:t-1}) = \delta(\mathbf{z}_{j,t} - \mathbf{z}_{j,t-1}), \quad (21)$$

$$\mathbf{z}_{j,t} = \mathbf{z}_{j,t-1}. \quad (22)$$

Noteworthy,  $p(\mathbf{z}_{j,t}|\mathbf{z}_{j,t-1}, \mathbf{D}_{1:t-1}, \mathbf{X}_{1:t-1})$  can be replaced by a motion estimator if a motion model is available. With (21) and (22), it follows

$$\begin{aligned} w_{j,t} &= \sum_{\mathbf{z}_{j,t-1}} (\bar{w}_{j,t-1} \delta(\mathbf{z}_{j,t} - \mathbf{z}_{j,t-1})) p(\mathbf{D}_t|\mathbf{z}_{j,t}, \mathbf{X}_t) \\ &= \bar{w}_{j,t-1} p(\mathbf{D}_t|\mathbf{z}_{j,t}, \mathbf{X}_t) \end{aligned} \quad (23)$$

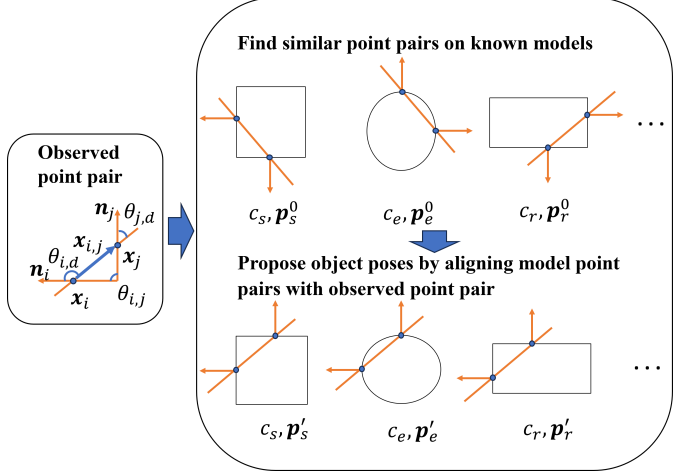


Fig. 2. An example of sampling particles with point-pair features. For each observed data point pair,  $\theta_{i,j}, \theta_{i,d}, \theta_{j,d}$  and  $\|\mathbf{x}_{i,j}\|_2$  are calculated as the point pair features.  $\mathbf{x}_{i,j}$  denotes the vector  $\mathbf{x}_j - \mathbf{x}_i$ .  $\theta_{i,j}, \theta_{i,d}, \theta_{j,d}$  are the angle between normal vectors of  $\mathbf{n}_i$  and  $\mathbf{n}_j$ , the angle between  $\mathbf{n}_i$  and  $\mathbf{x}_{i,j}$ , the angles between  $\mathbf{n}_j$  and  $\mathbf{x}_{i,j}$  respectively. Point pairs on all known models with similar features are extracted. Finally, by aligning known model point pairs with the observed point pair, possible combinations of the object class and object pose that match the observed point pair are found.  $c_s, c_e, c_r$  represent three object classes, namely square, ellipse, and rectangular respectively.  $\mathbf{p}_s^0, \mathbf{p}_e^0, \mathbf{p}_r^0$  are the original object pose (by convention set to  $[0, 0, 0, 0, 0, 0]$ ), whereas  $\mathbf{p}_s', \mathbf{p}_e', \mathbf{p}_r'$  are the pose after the alignment.

$$\bar{w}_{j,t} = \frac{w_{j,t}}{\sum_{j=1}^N w_{j,t}} \quad (24)$$

where  $\bar{w}_{j,t}$  is the normalized weight of particle  $\mathbf{z}_{j,t}$ . Note that the recursive formula of the particle weight update is consistent with (10).

As the particle filter needs to estimate the joint distribution of the object's class and its 6D pose, the number of particles required to cover the space sufficiently can be calculated as  $n \times m^6$ , where  $n$  denotes the number of known object classes, and  $m$  denotes the resolution of the discretization at each continuous dimension.

To enhance the sample efficiency of the particle filter and have better coverage on the high-density region of the posterior distribution, we propose to sample new particles based on newly observed data at each time step and mix them with existing particles. The rotation and translation invariant point-pair feature proposed in [4] is adopted for this purpose. For every two data points, the point-pair feature can be calculated. For more details about the alignment process, please refer to [4].

Fig. 2 illustrates the sampling procedure in a simplified 2D case. The same procedure holds for the 3D case, with more sophisticated objects.

For each known object, 200 feature points are sampled using Poisson Disc Sampling [31], resulting in  $200 \times 199 = 39800$  point pairs. The point-pair features for point pairs on known models are pre-computed, discretized and stored in a hash table for quick lookup at runtime. Each key in the table corresponds to a discretized feature value, and under the key is a list of point pairs on the known models that yield this discretized feature value. Each element in the list contains the indices of two points and their corresponding object class.

Upon a newly obtained contact point, new point-pair features between the new contact point and previous contact points are calculated, discretized, and used to look for point pairs on the known models with the same point-pair features using the hash table. The discretization is done by rounding  $\|\mathbf{x}_{i,j}\|_2$  to the closest one digit decimal and  $\theta_{i,j}, \theta_{i,d}, \theta_{j,d}$  to the closest multiple of 12 degrees. Importantly, the resolution of the discretization should be determined by the estimated noise level of the tactile signal, such that matches can be found during runtime. In the simulation, the noise level of the signal is known therefore it can be set directly. The lookup table process is used to find possible correspondence point pairs on known object models.

With the retrieved indices of points and their classes, their 3D coordinates and normal vectors can be obtained. Aligning the resulting model point pairs with newly observed point pairs yields potential combinations of object class and object pose that at least match one existing contact point pair. Given an observed point pair and a model point pair with point correspondences, a unique transformation can be derived to align two point pairs. For the alignment process, please see [4].

The lookup table and alignment processes together can be viewed as sampling particles from the mixture of posterior distributions  $p(\mathbf{z}|\mathbf{x}_i, \mathbf{n}_i, \mathbf{x}_j, \mathbf{n}_j)$  conditioned on each observed point pair. The core idea is that the sampling procedure can concentrate new particles in high probability density regions of the true posterior distribution which the PF aims to approximate.

As tactile data points are obtained sequentially in this study, at each time step  $t$ , new particles are sampled based on the new point-pair features. At time step  $t$ , if pairing the new contact point with all previously observed contact points  $t-1$ , the number of new point pairs is  $t-1$ , taking into the order of the points, in total  $2(t-1)$  pairs need to be considered, which is undesirable as  $t$  increases. Additionally, to assign proper weights to new particles, they need to be evaluated on previous observations and it is computationally expensive to evaluate all new particles on all previous observations.

To this end, we propose a method to select a fixed number of contact locations  $\mathbf{X}_s$  from  $\mathbf{X}_{1:t-1}$  at time step  $t$ , to form a fixed number of new point-pair features, while evaluating the new particles sampled from these features on the observed data  $\mathbf{D}_s$  at  $\mathbf{X}_s$ , as follows. A subset of previous observed tactile data  $\mathbf{D}_{1:t-1}$  at  $\mathbf{X}_{1:t-1}$  is selected to determine the relative weights among new particles within each object class. All previous contact locations in  $\mathbf{X}_{1:t-1}$  are first sorted based on their distance to the new observed contact location, and then the sorted contact locations are divided into  $n_s$  adjacent segments with the same size. The first point within each segment constitutes  $\mathbf{X}_s$ . The tactile data observed at  $\mathbf{X}_s$  is selected as  $\mathbf{D}_s$ . As a result, at each time step, a fixed number,  $2 \times n_s$  of new point-pairs are considered, as the order of points matters due to discretization. A fixed number  $n_s$  of points are used to calculate the relative weights. This choice is incentivized by locations with richer distance profiles that will capture the global context of the object better compared to using a temporal sliding window as proposed in [10].

The derivation of the weight approximation scheme goes as follows. Let us denote the weight of new particles  $\mathbf{z}'_{c,k,t}$  with class  $c$  by  $w'_{c,k,t}$  and the highest weight among them by  $w'_{c,*,t}$ .  $w'_{c,*,t}$  need to satisfy the following equation:

$$\frac{w'_{c,k,t}}{w'_{c,*,t}} = \frac{p(\mathbf{D}_s | \mathbf{z}'_{c,k,t}, \mathbf{X}_s)}{p(\mathbf{D}_s | \mathbf{z}'_{c,*,t}, \mathbf{X}_s)}. \quad (25)$$

For each object, class  $c$ ,  $\mathbf{z}'_{c,k,t}$  will be evaluated based on all previous observations  $\mathbf{D}_{1:t}$  at locations  $\mathbf{X}_{1:t}$  to determine its weight  $w'_{c,*,t}$  with respect to the weight of the old MLE particle  $\bar{w}^*$ . In other words,

$$\frac{w'_{c,*,t}}{\bar{w}^*} = \frac{p(\mathbf{D}_{1:t} | \mathbf{z}'_{c,*,t}, \mathbf{X}_{1:t})}{p(\mathbf{D}_{1:t} | \mathbf{z}^*, \mathbf{X}_{1:t})} \quad (26)$$

Combining (25) and (26),

$$w'_{c,k,t} = \frac{p(\mathbf{D}_s | \mathbf{z}'_{c,k,t}, \mathbf{X}_s)}{p(\mathbf{D}_s | \mathbf{z}'_{c,*,t}, \mathbf{X}_s)} \frac{p(\mathbf{D}_{1:t} | \mathbf{z}'_{c,*,t}, \mathbf{X}_{1:t})}{p(\mathbf{D}_{1:t} | \mathbf{z}^*, \mathbf{X}_{1:t})} \bar{w}^* \quad (27)$$

One key characteristic of this approximation is that  $w'_{c,k,t}$  can be higher than  $\bar{w}^*$  only if  $\mathbf{z}'_{c,k,t}$  is a better fit compared to  $\mathbf{z}^*$  over all observations  $\mathbf{D}_{1:t}$ .

To further reduce the computational cost, the proposed sampling scheme is only performed when the MLE model evidence  $p(\mathbf{D}_{1:t} | \mathbf{z}^*, \mathbf{X}_{1:t})$  smaller than a certain threshold  $\lambda$ . In other words, if the MLE is a good fit for the data, new particles will not be proposed.

The pseudo-code for the PF is shown in Algorithm 1. At each time step, a resampling step is carried out before sampling new particles from point-pair features to keep the total number of particles small. In this study, the stochastic universal sampling (SUS) is used. The SUS guarantees the survival of particles with normalized weights larger than  $\frac{1}{N}$ , when  $N$  is the number of samples to be drawn.

#### F. Discriminating Known and Unknown Objects

To discriminate between known and unknown objects, a threshold needs to be defined for the MLE model evidence  $p(\mathbf{D} | \mathbf{z}^*, \mathbf{X})$ . In this study, two types of data points are present, namely, contact points and non-contact points. The criterion for an object to be classified as a known object is defined as follows

$$p(\mathbf{D} | \mathbf{z}^*, \mathbf{X}) \geq \frac{1}{Z} (0.90)^{n_{pos}} * (0.50)^{n_{neg}}, \quad (28)$$

where  $n_{pos}$  denotes the number of observed contact points,  $n_{neg}$  denotes the number of observed non-contact points. Recall from (14) that, when a contact point is exactly on the estimated surface, its likelihood equals  $\frac{1}{Z}$ . The criterion encourages the average observation likelihood of contact points to be greater than or equal to 90 percent of the maximum likelihood of exact contact, while the average observation likelihood of the non-contact points to be greater than or equal to 0.5. If the observation likelihood for a non-contact point is below 0.5, it penetrates the MLE shape. The 0.5 likelihood threshold implies that the MLE shape should not be in penetration with the non-contact points for known objects.

**Algorithm 1:** Particle Filter (PF) for Object Recognition and Pose Estimation

---

$z_{j,t}$  := class and the pose of particle  $j$  at time step  $t$   
 $\bar{w}_{j,t}$  := normalized weight of particle  $j$  at time step  $t$   
 $D_t$  := the tactile data observed at time step  $t$   
 $X_t$  := the data point locations at time step  $t$   
 $T$  := total number of time steps  
 $S$  := the set of all particles in the PF  
**Initialization, when**  $t = 1$ :  
 Sample particles by aligning each feature point and its normal vector on known models with the first oriented contact point.  
 $S \leftarrow ((z_{1,1}, w_{1,1}), \dots, (z_{N,1}, w_{N,1}))$   
**for**  $t = 2, \dots, T$  **do**  
**for**  $(z_{j,t}, \bar{w}_{j,t}) \in S$  **do**  
     **Weight update:** Update the normalized weight  $\bar{w}_{j,t}$  for particle  $j$  based on (23) and (24)  
**end**  
**Resampling:**  
 $S \leftarrow$  Stochastic Universal Sampling(S)  
**Tracking model evidence:** Find the MLE particle  $(z^*, \bar{w}^*)$  based on (11) and calculate the model evidence  $p(D_{1:t}|z^*, X_{1:t})$   
**if**  $p(D_{1:t}|z^*, X_{1:t}) \leq \lambda$  **then**  
     **Sampling particles:** Sample new particles  $(z'_{k,t}, w'_{k,t})$  based on point-pair features of observed point pairs and (25)-(27), in total  $K$  particles are sampled.  
     **for**  $k = 1, \dots, K$  **do**  
          $S \leftarrow S \cup (z'_{k,t}, w'_{k,t})$   
     **end**  
**end**  
**end**

---

#### G. Gaussian Process Implicit Surface for Shape Reconstruction

When a novel object is detected, the Gaussian Process Implicit Surface (GPIS) [14] is used to reconstruct the shape given a prior function  $\mu$  and observed data  $D$ . The aim is to learn a signed distance function that fits the data  $D$  while taking into account the prior  $\mu$ . Similar to  $\hat{d}$  in (6),  $\mu : \mathbb{R}^3 \rightarrow \mathbb{R}^4$  maps a point  $x$  in the Euclidean space to a predictive signed distance value and a gradient vector.

Under the GP assumption, given an unexplored location  $x^*$ , observed contact points  $X$  and observed tactile data  $D$ , the predictive observation  $d^*$  at  $x^*$  satisfies,

$$d^*(x^*) \sim N(\mu^*(x^*), \Sigma^*(x^*)). \quad (29)$$

The mean  $\mu^*(x^*)$  and the covariance matrix  $\Sigma^*(x^*)$  are given by

$$\mu^*(x^*) = \mu(x^*) + k_*(K + \sigma^2 I)^{-1}(\bar{D} - \bar{\mu}(X)), \quad (30)$$

$$\Sigma^*(x^*) = k_{**} - k_*(K + \sigma^2 I)^{-1}k_*^T \quad (31)$$

where  $k_{**}$ ,  $k_*$  and  $K$  is the covariance matrix between  $(d^*, d^*)$ ,  $(d^*, D)$  and  $(D, D)$  respectively;  $\sigma$  denotes the

sensory noise level;  $\bar{D}$  represents a flattened vector that contains observed data  $D$  observed at  $X$ , while  $\bar{\mu}(X)$  represents a flattened vector that contains the prior predictive observed values at  $X$ . The covariance matrix between  $d$  at  $x$  and  $d'$  at  $x'$  can be calculated as

$$cov(d, d') = \begin{bmatrix} k_f(x, x') & \nabla_{x'} k_f(x, x') \\ \nabla_x k_f(x, x') & \nabla_{x'} \nabla_x k_f(x, x') \end{bmatrix}, \quad (32)$$

where  $k_f$  is the kernel function of choice. Following (32),  $k_{**}$ ,  $k_*$  and  $K$  can be calculated.

In this study, the thin-plate kernel [14] [21] is used. The thin-plate kernel function is defined as follows,

$$k_f(x, x') = k_{TP}(x, x') = a(2d^3 - 3Rd^2 + R^3) \quad (33)$$

$$d = \|x - x'\|_2 \quad (34)$$

The first and second derivatives of  $k_{TP}(x, x')$  can be calculated as

$$\frac{\partial k_{TP}(x, x')}{\partial x_i} = 6a(x_i - x'_i)(d - R), \quad (35)$$

$$\frac{\partial^2 k_{TP}(x, x')}{\partial x_i \partial x_j} = -6a \left( \frac{(x_i - x'_i)(x_j - x'_j)}{d} + \delta_{ij}(d - R) \right), \quad (36)$$

where  $\delta_{ij}$  denotes the Dirac delta function  $\delta(i - j)$ . Differing from the definition in [14] [21], a scaling coefficient  $a$  is introduced to allow the GP to adapt to different novel objects. The higher  $a$  is, the larger the assumed process noise is, which corresponds to assuming a larger difference between the prior and the actual object. The kernel parameter  $a$  can be updated online using a gradient-based optimizer to maximize the data likelihood of the GP [32]. Last but not least, only contact points are used to update the GP since the signed distance values at contact points are precise, while it is not the case for non-contact points.

#### H. Combining PF and GPIS

For GPIS reconstruction, given a fixed prior function  $\mu$ , the negative log-likelihood of observing data  $D$  at a set of points  $X$  satisfies the following relation:

$$-\ln p(D|X) \propto (\bar{\mu}(X) - \bar{D})^T K^{-1} (\bar{\mu}(X) - \bar{D}) \quad (37)$$

Assuming the prior function for the GP is determined by the latent variables  $z$ , one can choose the prior function by minimizing the log-likelihood function,

$$\operatorname{argmin}_z -\ln p(D, z|X) \propto (\bar{D}(z, X) - \bar{D})^T K^{-1} (\bar{D}(z, X) - \bar{D}), \quad (38)$$

where  $\bar{D}(z, X)$  denotes a flattened vector that contains the predictive observed signed distance values and normal vectors at locations  $X$ . Equation (38) takes a similar form to (16). The difference is that the diagonal matrix  $\Sigma$  is replaced with the inverse of the kernel matrix  $K^{-1}$ . The MLE particle from the PF has a straightforward interpretation: the combination of

object class and pose that minimizes the total square difference between the prediction and observation for all data points.

In the PF, with the known object assumption, there is no spatial correlation between data points. For the GPIS, the test object is assumed to be unknown, therefore spatial correlation stemming from the GPIS's smoothness assumption is necessary for inferring the signed distance values and the surface normal vectors at unexplored locations.

The GPIS provides the ability of adapting to, and learning, novel shapes, whereas the PF can find the maximum likelihood combination of known object class and poses based on the observed data. Therefore, we propose to use the MLE particles of the PF as a prior for GPIS shape reconstruction. In this manner, the GPIS has a more flexible, grounded prior selection process and the knowledge from known shapes can be transferred to learn new shapes.

It is worth pointing out that, the MLE prior is not guaranteed to be better than other arbitrary priors given that the real object can differ substantially from any known object, but it will always base its choice on its prior knowledge and the observed data.

### I. Active Data Acquisition

As tactile data points at each time step only cover a fraction of the object surface, active data acquisition is required to address the uncertainty and ambiguity due to incomplete information. The process is divided into two steps: target point selection and contact enforcement. The idea is to first determine a target point, and start exploration from the candidate target point until a contact point is found.

1) *Target Point Selection*: One way to select the target point is to calculate the posterior variance for each vertex on the reconstructed surface based on (31), then the point with the highest posterior variance will be selected as the target point  $\bar{x}_{t+1}$  for the next time step, i.e.,

$$\text{var}(\mathbf{x}^*) = \Sigma_{0,0}^* \quad (39)$$

$$\bar{x}_{t+1} = \underset{\mathbf{x}^* \in S^*}{\text{argmax}} \{ \text{var}(\mathbf{x}^*) \} \quad (40)$$

$$S^* \subset \{ \mathbf{x}^* \in R^3 \mid \mu^*(\mathbf{x}^*) = 0 \}, \quad (41)$$

with  $S^*$  a finite subset of the zero-level set of the posterior GPIS, which can be obtained through the marching cubes algorithm [33].

However, this exploration procedure requires the framework to update the GPIS every time step, which is computationally expensive. To alleviate this issue, the GPIS will not be updated and the framework will use the MLE shape from PF as estimated shape when the object is considered to be a known object. An exploration based on the directed Hausdorff distance (DHD) is used to guide the exploration as variance from the GPIS is not available. The point of interest for the next time step  $\bar{x}_{t+1}$  can be selected on the MLE surface by finding the point that yields the largest DHD, i.e.,

$$\bar{x}_{t+1} = \underset{\mathbf{x}_m \in M}{\text{argmax}} \underset{\mathbf{x}_c \in X_c}{\min} \|\mathbf{x}_m - \mathbf{x}_c\|_2, \quad (42)$$

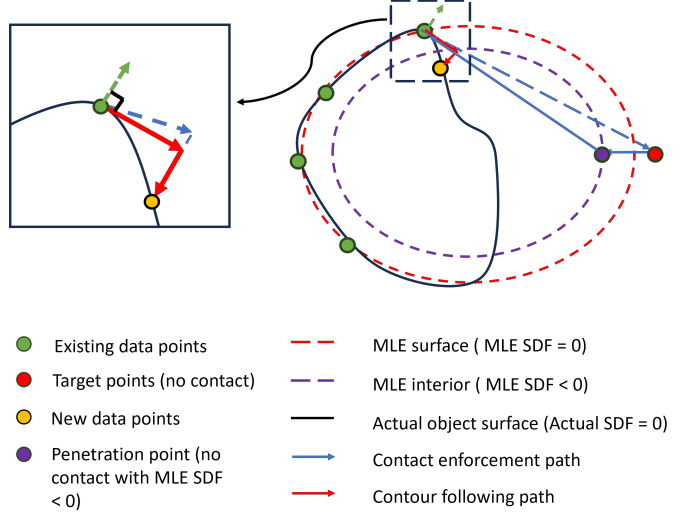


Fig. 3. Example of the contact enforcement procedure. Starting from the target point (red dot), the sensor first moves towards the interior of the MLE shape (purple dot). If no contact is found, the sensor moves towards the closest existing contact point (green dot). If no contact is established either, the closest known contact point is contacted again. From there, the algorithm takes small steps on the surface along the local tangent plane, towards the target point while remaining in contact with the surface. After a short distance, a new contact point will ultimately be recorded (yellow dot).

where  $M$  represents the set of all vertices of the MLE shape, and  $X_c$  denotes the set of observed contact points. The point of interest obtained through (42) is the point on the MLE shape with the largest distance to its nearest data point. And DHD is defined as follows,

$$d_H(\mathbf{A}, \mathbf{B}) = \max_{\mathbf{a} \in \mathbf{A}} \min_{\mathbf{b} \in \mathbf{B}} \|\mathbf{a} - \mathbf{b}\|_2 \quad (43)$$

where  $\mathbf{A}$  and  $\mathbf{B}$  are two point sets.

Both GPIS-based and DHD-based target point selection procedures share the same idea, prioritizing target points that are far away from existing data points in the hope of capturing the global context efficiently. In the following sections, the aforementioned target point selection procedure will be referred to as the GPIS-DHD exploration procedure.

2) *Contact Enforcement*: With equations (40) and (42), a candidate target point is obtained at each time step, but there is no guarantee that it would lead to contact. On the contrary, since the target point is near the furthest point on the estimated surface from the existing data point, it often fails to establish contact at the proposed target location. A simple solution to guarantee contact at each time step is to perform contour following, namely, the tactile sensor will move towards the target point locally on the tangent plane at each time step. However, this approach might take a long time to reach the target location and fail to capture the global context efficiently. As the selected target point is either on the GPIS or the MLE shape, confirming the occupancy near the target point can provide information that could greatly impact the belief of the framework. Negative information (non-contact points) around the target point implies the current estimation is likely to be wrong, whereas positive information (contact) provides evidence of the current estimation.

Fig. 3 sketches the contact enforcement procedure; see caption for details. During the contact enforcement procedure, most waypoints only contain negative information. Naively taking all the negative information data into account will lead to the negative information dominating the likelihood function, while the contact points would have less impact. To compensate for the imbalanced data issue, only target points that are far from the final contact points will be registered as negative information. In this manner, the number of data points that contain negative information is no larger than the number of data points with positive information.

Alternatively, when no prior is available, a rapidly exploring random tree (RRT) based exploration procedure can be adopted. It simply chooses a random point in the workspace, and it expands in that direction from the closest existing contact point. This requires no prior knowledge or estimation of the global shape as the expansion is local.

#### J. Termination criterion

In practice, the termination of the algorithm can be based on a time limit, e.g. the limit of registered data points. In this study, we define a termination criterion based on the DHD to ensure the framework terminates if, and only if, enough information is obtained on the object's surface. The incentive behind this choice of criterion is to make the framework decide when to terminate based on the data point's coverage on the object's surface. For known objects, the termination criterion can be written as

$$d_H(\mathbf{M}, \mathbf{X}_c) \leq \epsilon \quad (44)$$

The algorithm terminates if  $d_H(\mathbf{M}, \mathbf{X}_c)$  is lower than a small value  $\epsilon$ , where  $\mathbf{M}$  represents the set of all vertices of the MLE shape, and  $\mathbf{X}_c$  denotes the set of observed contact points. Intuitively, if any point on the estimated surface is at most  $\epsilon$  away from its closest existing contact point, the program terminates. In other words, to terminate the exploration, the contact points have to cover the estimated object surface with a certain density related to  $\epsilon$ . The threshold  $\epsilon$  can be interpreted as a level of detail parameter: lower  $\epsilon$  results in more data being collected, albeit with longer exploration time. Similarly, for novel objects, the termination criterion is

$$d_H(\mathbf{S}^*, \mathbf{X}_c) \leq \epsilon, \quad (45)$$

with  $\mathbf{S}^*$  as the zero level set of the GPIS. Although the posterior variance of the GPIS can also be used for the same purpose, the proposed criterion  $d_H(\mathbf{S}^*, \mathbf{X}_c)$  has the advantage of being independent of the choice of kernel parameters of the Gaussian process and the type of test objects at hand. With all the components defined, the pseudo code for the active tactile perception framework is given in Algorithm 2.

#### K. Shape similarity metric

In this study, the two-way Hausdorff distance (TWD) is used to measure the difference between two shapes:

$$d_{TH}(\mathbf{A}, \mathbf{B}) = \max(d_H(\mathbf{A}, \mathbf{B}), d_H(\mathbf{B}, \mathbf{A})) \quad (46)$$

This metric is used in the evaluation of the proposed framework. The pose estimation error is measured by the TWD

---

#### Algorithm 2: Bayesian framework for object recognition, pose estimation and shape reconstruction

---

**Initialization:** Initialize the particle filter with the first contact point  $\mathbf{x}_1$  and tactile observation  $\mathbf{d}_1$ .

**while**  $d_H(\mathbf{S}^*, \mathbf{X}_c) > \epsilon$  **do**

- Update belief using the particle filter, extract the MLE particle  $(\mathbf{z}^*, \bar{w}^*)$  and its model evidence  $p(\mathbf{D}|\mathbf{z}^*, \mathbf{X})$
- if**  $p(\mathbf{D}|\mathbf{z}^*, \mathbf{X}) < (\frac{1}{Z}0.90)^{n_{pos}} * (0.50)^{n_{neg}}$  **then**

  - Update GPIS and select the next target point  $\bar{\mathbf{x}}_{t+1}$  from the zero level set of GPIS  $\mathbf{S}^*$  using eq. (40)

- else**

  - Select the next target point  $\bar{\mathbf{x}}_{t+1}$  from the set of MLE surface  $\mathbf{M}$  using eq. (42)

- end**
- Establish contact using the exploration procedure and add data points to  $\mathbf{X}$  and data to  $\mathbf{D}$ .
- Update  $d_H(\mathbf{S}^*, \mathbf{X}_c)$  based on eq. (43)

**end**

---

between the MLE shape from the PF and the actual shape of the test object. Similarly, the shape reconstruction error is measured by the TWD distance between the reconstructed shape from the GPIS and the actual shape of the test object.

## IV. EXPERIMENTS

#### A. Experiment setup

To show that the framework can address both known and unknown objects, we selected ten 3D models from the Princeton Shape Benchmark [34] and the Stanford 3D Scanning Repository [35] as known objects, and ten comparable, but distinct, other objects from the same databases as novel objects. They are all scaled to fit in a  $6 \times 6 \times 6$  bounding box. This should make it less likely for the framework to identify the correct object class merely by the length of the object. For this reason, the distance unit in this study does not correspond to real world measurements. An overview of the objects used in the experiments are shown in Fig. 4 and 5. Both known and novel objects are used as test objects in the experiment. For each



Fig. 4. The ten known objects used in the experiments. From left to right, top to bottom, the objects are named as armadillo, asian dragon, elephant, bottle 1, mug 1, ice cream 1, guitar 1, vase 1, office chair and sofa 1 respectively.

trial in the experiment, a test object is initialized with a random



Fig. 5. The ten novel objects used in the experiments. From left to right, top to bottom, the objects are neptune, dragon, noisydino, bottle 2, mug 2, ice cream 2, guitar 2, vase 2, home chair and sofa 2 respectively.

pose and assumed to stay in that fixed position during the experiment. Once the first contact is established, the robotic arm will start to explore the object surface actively with the proposed exploration procedure, while updating its belief of the object class and object pose, and constantly reconstructing the shape until the termination criterion is satisfied. To explore the performance of the framework, ten trials are carried out per test objects. As performance indices we record object class prediction error, pose estimation error, reconstruction error, and termination time step.

Furthermore, to demonstrate the effectiveness of the proposed exploration procedure with the GPIS-DHD, this method is compared to the RRT-based exploration procedure.

In all experiments, the same hyper-parameter values are used as listed in Table I. The values of  $\sigma_d$  and  $\sigma_n$  are tuned to the known object sets. While sensory noise  $\sigma$  is set based on the zero level set error tolerance of the simulator, the initial value of  $a$  denoted as  $a_0$  is set to 1 for convenience as it will be optimized online.

TABLE I  
PARAMETER SETTINGS.

parameter	$\sigma_d$	$\sigma_n$	$\sigma$	$a_0$	$\epsilon$	$n_s$	$\lambda$
value	0.50	1.50	$1.00 \times 10^{-4}$	1.00	0.60	30	0.97

## B. Results

For clarity, the analysis of the results are separated for known test objects and novel test objects. For known objects, pose error is measured by the TWD distance between the vertices of the MLE shape  $M$  and the vertices of the ground truth object shape  $M$ . Similarly, for novel objects, the reconstruction error is measured by the TWD between the vertices of the GPIS  $S^*$  and the vertices of the ground truth object shape  $M$ . The surface uncertainty for both known and novel object is instead measured by the DHD between  $M$  and all contact points  $X_c$ . An overview of the results for the experiments can be found in Fig. 6.

1) *Object recognition and pose estimation with known objects:* When addressing known objects, regardless of the choice of exploration procedure, the framework correctly identified the class of the objects in all 100 trials and achieved

pose estimation errors below the desired threshold of 0.6 in 100 out of 100 trials.

As shown in Fig. 6a, averaging over all runs, pose estimation error drops to the desired level (0.6) within approximately 20 time steps, regardless of the choice of exploration procedure. On the other hand, Fig. 6c indicates the GPIS-DHD exploration procedure achieved a much faster coverage of the object surface than the RRT-based exploration procedure, with roughly 50 vs 200 time steps on average. It is reflected in Fig. 6d that the GPIS-DHD exploration procedure had a clear advantage of satisfying the coverage-based termination criterion sooner, compared to the RRT-based exploration procedure for all known objects. Noteworthy, for the experiment with the RRT-based exploration procedure, the PF estimated the object class and object pose accurately, even though the object surface was not fully explored at the early stage of the exploration. This shows that the PF can effectively distinguish the known objects effectively in the priors with partial information.

Fig. 6b shows that the GPIS-DHD exploration had a small lead in reaching the desired pose estimation error in 9 out of 10 classes, while having a major lead in the class mug 1, compared to the RRT-based exploration procedure. With Fig. 7, one can see there is a clear difference of the pose estimation error over time between the two exploration procedures for the mug 1 class. To distinguish the pose of the mug, its handle must be located to break the rotational symmetry of its main body. The RRT-based exploration procedure on average took longer to locate the mug's handle compared to the GPIS-DHD exploration procedure. The visualization of this special case can be found in Fig. 8.

2) *Sampling efficiency of the particle filter:* To demonstrate the sampling efficiency of our particle filter, we tracked the number of particles during the GPIS-DHD object recognition and pose estimation experiments. The largest number of particles observed at any time step over 100 runs was 6917, for representing the distribution of 10 object classes and the pose of the object.

3) *Shape reconstruction with unknown objects:* When addressing a novel object, the framework reconstructed the novel shape with decreasing reconstruction error as more data points were collected, as shown in Fig. 6e. Utilizing the GPIS-DHD exploration procedure yielded lower reconstruction error, on average, than using the RRT exploration procedure. Fig. 6f gives more details on the number of time steps taken to achieve the desired reconstruction error for each novel object class. For most classes, GPIS-DHD outperformed the RRT-based exploration procedure. In addition, the GPIS-DHD exploration procedure achieved faster global coverage of the object surface in comparison with the RRT-based exploration procedure, as shown in Fig. 6g. This is also reflected in Fig. 6h, as the GPIS-DHD exploration procedure terminated sooner than the RRT-based exploration procedure on average for most objects in the novel object set. Comparing Fig. 6d and 6h, the average number of time steps taken to explore the novel object variants are similar to their corresponding original known objects. Noteworthy, two novel objects, ice cream 2 and guitar 2, are classified as known objects. Though they are visually different from ice cream 1 and guitar 1 respectively, as can be seen

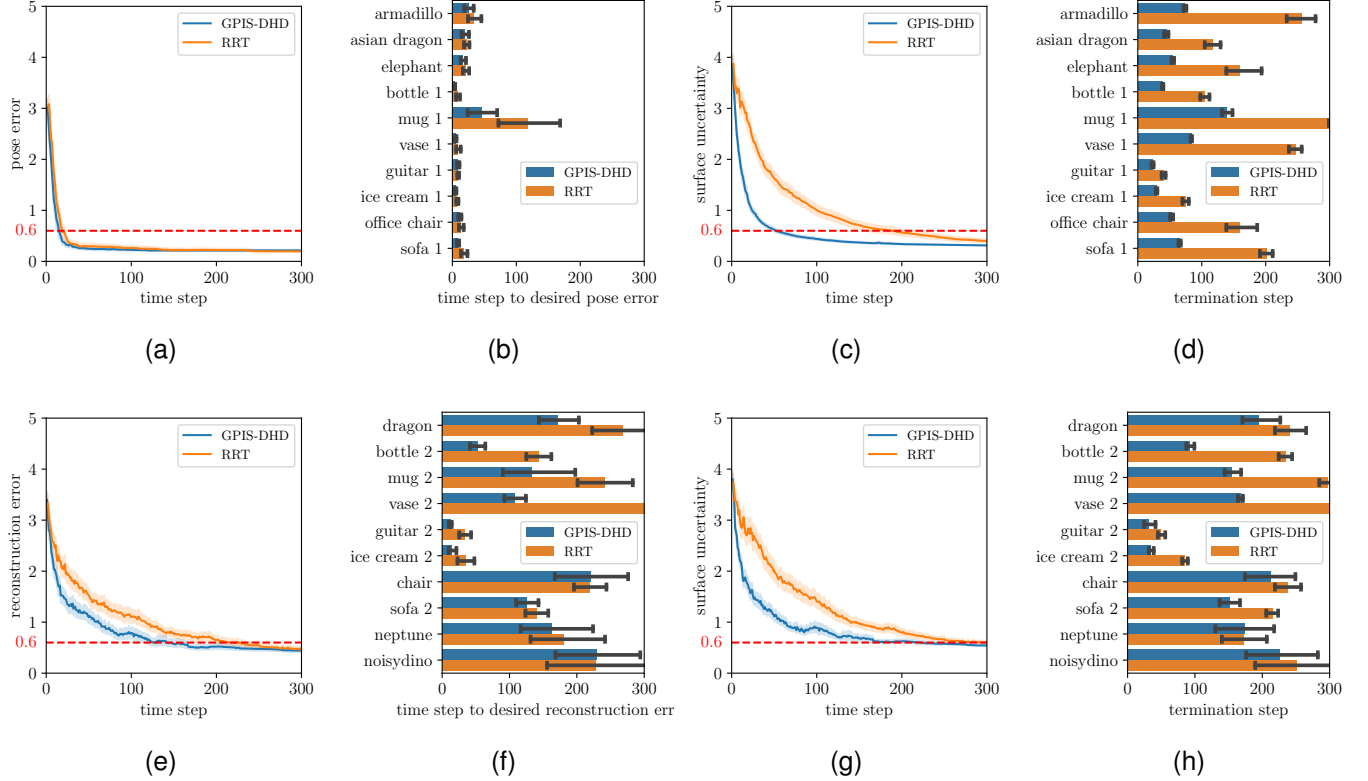


Fig. 6. An overview of simulation experiment results, the first row is for known objects and the second row is for novel objects: (a) Average pose estimation error over time with GPIS-DHD and RRT-based exploration procedures for known objects. The orange and blue line indicate the mean pose error at each time step over 100 trials for the ten known objects. The red dashed line indicates the desired pose error threshold. (b) The time steps to reach below 0.6 pose error for each known object class. (c) Average DHD from MLE to contact data points over time with GPIS-DHD and RRT-based exploration procedures. The DHD from MLE shape to contact data points is used to determine if the contact data points cover the estimated surface sufficiently. The red dashed line indicates the DHD threshold for termination. (d) Termination time steps for known objects with GPIS-DHD and RRT-based exploration procedures. (e) Average shape reconstruction error for novel objects with GPIS-DHD and RRT-based exploration procedures for unknown objects. The red dashed line indicates the desired reconstruction error threshold. (f) The time steps to reach below 0.6 reconstruction error for each novel object class. (g) Average DHD from MLE to contact data points over time with GPIS-DHD and RRT-based exploration procedures for unknown objects. The DHD from GPIS to contact data points is used to determine if the contact data points cover the estimated surface sufficiently. The red dashed line indicates the DHD threshold for termination. (h) Termination time step for novel objects with GPIS-DHD and RRT-based exploration procedures. The translucent bands around the curves in (a) (c) (e) (g) and the error bars in (b) (d) (f) (h) indicate the confidence interval of 95%.

in Fig. 4 and Fig 5, the differences were not large enough to be identified as novel objects. In these two cases, GPIS reconstruction was not performed as they were regarded as known objects by the framework. Combining Fig. 6b, 6d, 6f and 6h, it can be derived that unlike estimating the pose of a known object, to reach the desired level of reconstruction error for a novel object requires more time steps and better coverage of the surface on average.

Table II summarizes the statistics of the reconstruction error for each class. Each column reports the statistics of the TWD between the corresponding method and the ground truth shape. MLE shape denotes using the MLE prior from PF as the reconstructed shape, GPIS with MLE prior denotes our method, and Poisson surface denotes the Screened Poisson reconstruction method [31] (depth = 9). As ice cream 2 and guitar 2 were regarded as known object by the framework, their GPIS results were not available, denoted with N/A. The same data were used for the GPIS and the Poisson surface reconstruction, which are the oriented point clouds acquired from the GPIS-DHD exploration experiments. In our experiment, the GPIS with MLE prior yields, in most cases, lower reconstruction

error than the Poisson surface reconstruction.

A few examples of GPIS shape reconstruction with MLE shape priors can be seen in Fig 9. As can be seen, the proposed framework made sensible choices of the MLE priors and the GPIS reconstruction program did well in closing the gap between the MLE priors and the ground truth shapes.

*4) Including learned shapes as priors:* To demonstrate the learning capability of the framework, we included the learned chair model as a new prior and then performed experiments with the chair object in different poses. In total, 10 trials were carried out. The results are shown in Figs. 10, 11a and 11b. The framework successfully recognized the chair and estimated its poses accurately within 50 time steps. In 10 trials, the exploration terminated within 90 time steps; on average it took approximately 68 steps to finish the exploration, which is much faster compared to over 200 steps before adding the learned chair prior, as can be inferred from Figs. 11b and 6h.

The results show that the framework can learn new object shapes through shape reconstruction and utilize the knowledge effectively for object recognition and pose estimation, even though the learned shape is not identical to the actual object.

TABLE II  
COMPARISON OF TWO SHAPE RECONSTRUCTION METHODS

class	TWD/reconstruction error					
	MLE shape		GPIS with MLE prior		Poisson surface	
mean	std	mean	std	mean	std	
bottle 2	0.994	0.088	<b>0.259</b>	<b>0.036</b>	0.416	0.063
dragon	2.952	0.133	<b>0.478</b>	<b>0.057</b>	0.582	0.122
guitar 2	<b>0.412</b>	<b>0.062</b>	N/A	N/A	1.092	0.673
chair	1.771	<b>0.085</b>	<b>0.505</b>	0.402	1.054	0.360
ice cream 2	<b>0.432</b>	<b>0.046</b>	N/A	N/A	0.546	0.126
mug 2	0.580	<b>0.129</b>	<b>0.526</b>	0.335	1.703	0.282
neptune	1.735	0.801	<b>0.505</b>	<b>0.125</b>	0.655	0.201
noisydino	1.053	0.106	<b>0.519</b>	<b>0.089</b>	0.518	0.152
sofa 2	0.611	0.049	<b>0.483</b>	<b>0.043</b>	0.604	0.045
vase 2	1.453	0.221	<b>0.335</b>	<b>0.060</b>	0.658	0.081

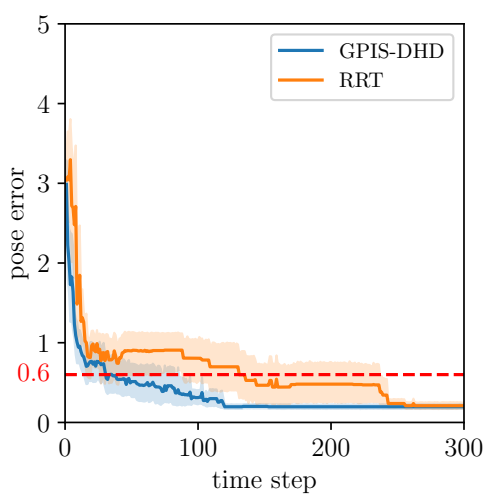


Fig. 7. Average pose estimation error for mug 1 over time with GPIS-DHD and RRT-based exploration procedures. The GPIS-DHD procedure achieves the desired pose estimation error faster compared to the RRT-based procedure. The translucent bands around the curves indicate the confidence interval of 95%.

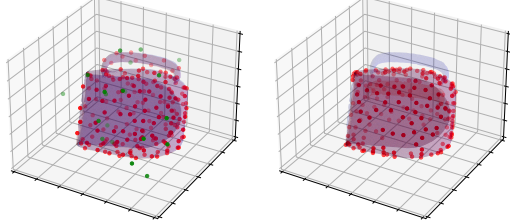


Fig. 8. Comparison of the mug 1 case with GPIS-DHD and RRT exploration procedures respectively: On the left, GPIS-DHD exploration procedure managed to cover the mug's handle after 200 contact points (red dots), therefore the ground truth (blue shape) and the MLE shape (red shape) overlapped. On the right, RRT exploration procedure failed to find the handle after 200 contact points, therefore lacked information to determine the mug's pose.

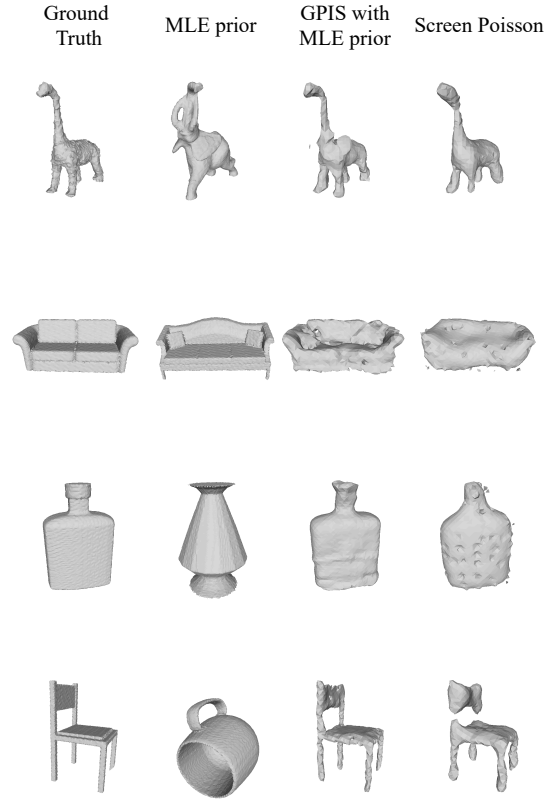


Fig. 9. Examples of the maximum likelihood estimation (MLE) priors and reconstructed surfaces in the experiments. Each row is one experiment. From left to right, the first column shows the ground truth object shape, the second column shows the MLE shape from the particle filter (PF), the third column shows the Gaussian process implicit surface (GPIS) reconstructed using the MLE shape as prior, the last column shows the reconstructed result using the Screened Poisson surface reconstruction.

## V. DISCUSSION

### A. Object recognition and pose estimation for known objects

In this work, we presented a Bayesian framework for robotic arm control that can efficiently identify objects from their shape and poses. Moreover, we showed knowledge transfer from known shapes to actively learn novel objects' shapes of previously unfamiliar objects. Accordingly, adding the newly learned shape of the novel object lead to the prior being extended with a new object class that made the robotic arm

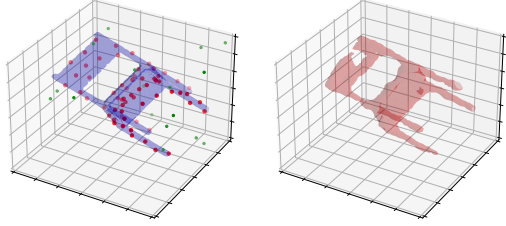


Fig. 10. An example of including a learned shape as a prior of the framework: After including the learned chair shape as a prior, the framework successfully recognized the chair (blue shape) as the learned reconstructed model (red shape).

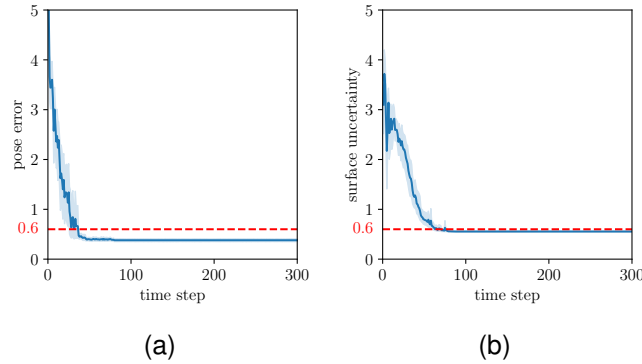


Fig. 11. (a) Average pose estimation error over 10 trials in the learned chair prior experiment. The red dashed line indicates the pose error threshold. (b) Average DHD error 10 trials in the learned chair prior experiment. The red dashed line indicates the DHD threshold for termination. The translucent bands around the curves in (a) (b) indicate the confidence interval of 95%.

identically successful in recognising objects in consequent trials. In order to do so, we formulated object recognition, shape and pose estimation with touch as a non-linear Bayesian filtering problem and adopted a particle filter-based approach (PF).

Compared to Kalman Filters, PFs can approximate arbitrary distributions, which is needed to capture the ambiguity and uncertainty present due to partial tactile observations. Our PF uses a sampling procedure based on point-pair features and a custom weight assigning scheme to achieve efficient estimations of the joint distribution of object class and object pose estimation. We estimated the joint distribution of object class and object pose for ten object classes with less than 7000 particles, thus 700 particles on average per object. It is worth pointing out that the core idea behind the sampling procedure is to use translation and rotation invariant features, in our case, distances and angles, to find possible point correspondences, and then use the point correspondences to solve for the potential object poses, making it far more efficient than considering single points. This idea is not limited to the point-pair feature. For instance, three or four points could be considered simultaneously. Nonetheless, a set of two points is chosen in this study because the alignment of two oriented point pairs can uniquely determine the pose while the number of all point pair combinations is tractable. If more than two points per set are considered simultaneously, the number of possible

combinations quickly becomes intractable. Similarly, in the sampling scheme, each object was represented by 200 points to keep the number of combinations tractable. Increasing the number of points will likely make the framework achieve the desired pose error sooner but at the cost of more computational resources.

In the object recognition and pose estimation experiment with known objects, the framework recognized the correct object class and achieved desired pose estimation error with a small amount of data points regardless of the selected exploration procedure. Both the GPIS-DHD and RRT-based exploration procedure worked well, however GPIS-DHD generally covered the estimated surface faster than the RRT-based exploration procedure. For most known objects used in the experiment, data points covering only a fraction of the object surface were sufficient to infer the correct object class and object pose. The exception was the mug shown in Fig. 8, for which the rotational symmetry of its main body caused the pose to only be resolved by finding its handle. Compared to the RRT-based exploration procedure, the GPIS-DHD exploration procedure tries to actively touch the region on the estimated shape that is far away from existing data points. When the mug's main body is covered by some data points, the handle of the estimated mug will be targeted more quickly. By confirming or failing to establish contact at the target location, the framework updates its belief of the handle location. In this case, the GPIS-DHD exploration procedure generated no-contact points during exploration, which was not the case for the RRT-based exploration procedure, since moving along the surface in small steps from a point on the surface guaranteed contact. The non-contact points in the GPIS-DHD played a crucial role in finding the mug's handle, as it provided information to narrow down where the handle was located. The proposed DHD termination made sure that the exploration would continue until the handle was found, as failing to establish contact on the handle would result in a large DHD from the estimated surface to data points, thereby failing to fulfill the termination criterion.

### B. Shape reconstruction for novel objects

The PF can identify unknown objects but lacks the ability to learn new shapes, so the GPIS is introduced to perform shape reconstruction. Aiming to exploit the prior knowledge, in this study, we initiate the prior of the GPIS to be the MLE shape from the PF. Our results showed that GPIS with MLE priors worked effectively with the novel object set and it achieved better performance than the screened Poisson surface reconstruction with the sparse point clouds from the GPIS-DHD exploration procedure. However, as the number of data points becomes denser, we expect the Poisson surface reconstruction may perform better than the GPIS with MLE priors, as the advantage of having a good prior decays as more data points are collected. In addition, dense point clouds can bring the covariance matrix (thin-plate kernel) of the GPIS closer to singularity and can potentially lead to broken surfaces. When observing Figs. 6d and 6h, it becomes clear that, in general, the framework took longer to explore a novel

object than a known object. That is partly due to the greater applicability of the prior knowledge for known objects than for novel objects. In fact, if the object does not deviate enough from all known objects, it would be recognized as a known object. As was the case for Ice cream 2 and guitar 2 in our set. The active tactile exploration for these two objects were merely slightly slower than the known Ice cream 1 and Guitar 1 respectively. We assumed the success of the GPIS with sparse data stemmed from good priors, and we expected the GPIS to under-perform when no good priors were available. Surprisingly, in some cases, e.g., the dragon class in Table II, showed that despite the large discrepancy between the MLE prior and the ground truth, the GPIS still performed well and achieved low reconstruction error. One potential reasoning behind this observation is that even if the MLE shape is not a good fit globally, parts of it could have similar features to the actual shape. The locally similar parts were kept, and taken advantage of, whereas the mismatched parts were corrected by the GPIS.

### C. Computational cost

When it comes to computational complexity, the PF's computational cost scales linearly with the number of observations, because the PF's weight assignment scheme for newly sampled particles requires the evaluation of one particle per class on all previous observations. Since the prior of the GPIS can be different at each time step, sparse GP with inducing points [36], [37] is not directly applicable, and the GPIS becomes computationally expensive as more data points are collected due to its  $O(N^3)$  complexity. One potential way to reduce the computational cost of the GPIS is to fix the prior after a certain amount of data, or when a certain level of surface coverage is reached, such that sparse GP becomes applicable. Moreover, as shown in the results section, new shapes can be learned and added as new priors to the framework, however, it will require proportionally more memory and computational time as the number of priors (here shape primitives) increases. Addressing these computational challenges would be one direction of future work. In this paper, the disadvantage of the increasing computational cost over time was partially compensated by the use of the proposed exploration procedure and the termination criterion. Noteworthy, though the proposed DHD threshold termination criterion was used in our experiments, it is by no means compulsory. A low DHD threshold can lead to a larger number of data points with better coverage of the object surface, while a high DHD threshold can allow faster conclusions but with higher chances of errors. A trade-off has to be made to determine a proper threshold value. However, the DHD from the estimated shape to existing data points could be viewed as a measure for the lowest data point density on the estimated object surface. In the case where another termination criterion applies, the DHD would still provide valuable information about how well the surface is covered, and the PF and GPIS can still output meaningful distribution on the object class, object pose, and estimated shape. Being uncertainty-aware of the coverage of the surface is one of the advantages of the proposed Bayesian framework.

### D. Limitations and future work

As can be seen in the results of GPIS reconstruction result, there were defects such as small holes on thin surfaces and disconnected small parts. These defects were not repaired in the current framework, and this was reflected in the reconstruction error. Addressing these undesired defects from the learned models will be valuable future work. In addition, as the framework assumes no movement nor multiple objects in the scene, lifting these assumptions will be another potential work direction. Moreover, in this study, the framework determined if an object was known or novel based on the proposed MLE model evidence from the PF. As this threshold for the decision can vary, it provides some flexibility in choosing how similar the object should be to be classified as an known object. Ideally, classification should also take into account the topology of shapes, therefore this could also be a topic for future investigation. Last but not least, the experiments of this study were only performed in simulation as a proof of concept and to introduce the framework, however, validation with a robot hardware setup will be left as future work.

## VI. CONCLUSION

In this paper, we proposed a Bayesian framework for active tactile object recognition, pose estimation, and shape reconstruction for motion planning of a robotic arm. The framework can utilize its prior knowledge to explore, recognize and localize known objects, and it can transfer the prior knowledge to learn shapes of novel objects. A GPIS-DHD exploration procedure and a DHD-based termination criterion were proposed to guide the active data acquisition process with success. In the experiments, we showed that the proposed framework along with the proposed exploration procedure were effective in the task of object recognition, pose estimation and shape reconstruction for both known and novel objects. To further demonstrate the learning capability of the framework, a newly learned object shape was added to the prior of the framework as a new object class and followingly, the framework successfully recognized the new object that it had learned from a previous trial through active tactile exploration.

## ACKNOWLEDGMENT

## REFERENCES

- [1] I. Taylor, S. Dong, and A. Rodriguez, "GelSlim3. 0: High-Resolution Measurement of Shape, Force and Slip in a Compact Tactile-Sensing Finger," *arXiv preprint arXiv:2103.12269*, 2021.
- [2] M. Lambeta, P.-W. Chou, S. Tian, B. Yang, B. Maloon, V. R. Most, D. Stroud, R. Santos, A. Byagowi, G. Kammerer, D. Jayaraman, and R. Calandra, "DIGIT: A Novel Design for a Low-Cost Compact High-Resolution Tactile Sensor with Application to In-Hand Manipulation," *IEEE Robotics and Automation Letters*, vol. 5, no. 3, pp. 3838–3845, Jul. 2020.
- [3] M. C. Koval, N. S. Pollard, and S. S. Srinivasa, "Pose estimation for planar contact manipulation with manifold particle filters," *The International Journal of Robotics Research*, vol. 34, no. 7, pp. 922–945, 2015.
- [4] B. Drost, M. Ulrich, N. Navab, and S. Ilic, "Model globally, match locally: Efficient and robust 3D object recognition," in *2010 IEEE Computer Society Conference on Computer Vision and Pattern Recognition*, Jun. 2010, pp. 998–1005.

[5] J. Elfring, E. Torta, and R. van de Molengraft, "Particle Filters: A Hands-On Tutorial," *Sensors*, vol. 21, no. 2, p. 438, Jan. 2021.

[6] M. Kaboli, K. Yao, D. Feng, and G. Cheng, "Tactile-based active object discrimination and target object search in an unknown workspace," *Autonomous Robots*, vol. 43, no. 1, pp. 123–152, Jan. 2019.

[7] M. Kaboli, D. Feng, K. Yao, P. Lanillos, and G. Cheng, "A Tactile-Based Framework for Active Object Learning and Discrimination using Multimodal Robotic Skin," *IEEE Robotics and Automation Letters*, vol. 2, no. 4, pp. 2143–2150, Oct. 2017.

[8] D. Xu, G. E. Loeb, and J. A. Fishel, "Tactile identification of objects using Bayesian exploration," in *2013 IEEE International Conference on Robotics and Automation*. Karlsruhe, Germany: IEEE, May 2013, pp. 3056–3061.

[9] A. Petrovskaya and O. Khatib, "Global Localization of Objects via Touch," *IEEE Transactions on Robotics*, vol. 27, no. 3, pp. 569–585, Jun. 2011.

[10] G. Vezzani, U. Pattacini, G. Battistelli, L. Chisci, and L. Natale, "Memory Unscented Particle Filter for 6-DOF Tactile Localization," *IEEE Transactions on Robotics*, vol. 33, no. 5, pp. 1139–1155, Oct. 2017.

[11] G. Vezzani, N. Jamali, U. Pattacini, G. Battistelli, L. Chisci, and L. Natale, "A novel Bayesian filtering approach to tactile object recognition," in *2016 IEEE-RAS 16th International Conference on Humanoid Robots (Humanoids)*. IEEE, Nov. 2016, pp. 256–263.

[12] S. Sun and B.-C. Min, "Active Tapping via Gaussian Process for Efficient Unknown Object Surface Reconstruction," Oct. 2021.

[13] N. Jamali, C. Ciliberto, L. Rosasco, and L. Natale, "Active perception: Building objects' models using tactile exploration," in *2016 IEEE-RAS 16th International Conference on Humanoid Robots (Humanoids)*. IEEE, Nov. 2016, pp. 179–185.

[14] O. Williams and A. Fitzgibbon, "Gaussian process implicit surfaces," in *Gaussian Processes in Practice*, 2006.

[15] M. Meier, M. Schopfer, R. Haschke, and H. Ritter, "A probabilistic approach to tactile shape reconstruction," *IEEE Transactions on Robotics*, vol. 27, no. 3, pp. 630–635, 2011.

[16] S. Dragiev, M. Toussaint, and M. Gienger, "Uncertainty aware grasping and tactile exploration," *Proceedings - IEEE International Conference on Robotics and Automation*, pp. 113–119, 2013.

[17] M. Li, K. Hang, D. Kragic, and A. Billard, "Dexterous grasping under shape uncertainty," *Robotics and Autonomous Systems*, vol. 75, pp. 352–364, Jan. 2016.

[18] D. Driess, P. Englert, and M. Toussaint, "Active learning with query paths for tactile object shape exploration," in *2017 IEEE/RSJ International Conference on Intelligent Robots and Systems (IROS)*. IEEE, Sep. 2017, pp. 65–72.

[19] D. Driess, D. Hennes, and M. Toussaint, "Active Multi-Contact Continuous Tactile Exploration with Gaussian Process Differential Entropy," in *2019 International Conference on Robotics and Automation (ICRA)*, May 2019, pp. 7844–7850.

[20] S. Dragiev, M. Toussaint, and M. Gienger, "Gaussian process implicit surfaces for shape estimation and grasping," in *2011 IEEE International Conference on Robotics and Automation*, May 2011, pp. 2845–2850.

[21] W. Martens, Y. Poffet, P. R. Soria, R. Fitch, and S. Sukkarieh, "Geometric Priors for Gaussian Process Implicit Surfaces," *IEEE Robotics and Automation Letters*, vol. 2, no. 2, pp. 373–380, Apr. 2017.

[22] A. Schneider, J. Sturm, C. Stachniss, M. Reisert, H. Burkhardt, and W. Burgard, "Object identification with tactile sensors using bag-of-features," in *2009 IEEE/RSJ International Conference on Intelligent Robots and Systems*, Oct. 2009, pp. 243–248.

[23] Z. Yi, R. Calandra, F. Veiga, H. van Hoof, T. Hermans, Y. Zhang, and J. Peters, "Active tactile object exploration with Gaussian processes," in *2016 IEEE/RSJ International Conference on Intelligent Robots and Systems (IROS)*, Oct. 2016, pp. 4925–4930.

[24] S. Yang, S. Jeon, and J. Choi, "Level-Set Based Greedy Algorithm With Sequential Gaussian Process Regression for Implicit Surface Estimation," in *ASME 2016 Dynamic Systems and Control Conference*. American Society of Mechanical Engineers Digital Collection, Feb. 2017.

[25] T. Matsubara and K. Shibata, "Active tactile exploration with uncertainty and travel cost for fast shape estimation of unknown objects," *Robotics and Autonomous Systems*, vol. 91, pp. 314–326, May 2017.

[26] M. Comi, Y. Lin, A. Church, A. Tonioni, L. Aitchison, and N. F. Lepora, "TouchSDF: A DeepSDF approach for 3D shape reconstruction using vision-based tactile sensing," Nov. 2023. [Online]. Available: <http://arxiv.org/abs/2311.12602>

[27] S. Wang, J. Wu, X. Sun, W. Yuan, W. T. Freeman, J. B. Tenenbaum, and E. H. Adelson, "3D Shape Perception from Monocular Vision, Touch, and Shape Priors," in *2018 IEEE/RSJ International Conference on Intelligent Robots and Systems (IROS)*, Oct. 2018, pp. 1606–1613.

[28] L. Rustler, J. Matas, and M. Hoffmann, "Efficient Visuo-Haptic Object Shape Completion for Robot Manipulation," in *2023 IEEE/RSJ International Conference on Intelligent Robots and Systems (IROS)*. Detroit, MI, USA: IEEE, Oct. 2023, pp. 3121–3128.

[29] E. Smith, R. Calandra, A. Romero, G. Gkioxari, D. Meger, J. Malik, and M. Drozdzal, "3D Shape Reconstruction from Vision and Touch," in *Advances in Neural Information Processing Systems*, vol. 33. Curran Associates, Inc., 2020, pp. 14193–14206.

[30] E. Smith, D. Meger, L. Pineda, R. Calandra, J. Malik, A. Romero Sorian, and M. Drozdzal, "Active 3D Shape Reconstruction from Vision and Touch," in *Advances in Neural Information Processing Systems*, vol. 34. Curran Associates, Inc., 2021, pp. 16064–16078.

[31] M. Kazhdan and H. Hoppe, "Screened poisson surface reconstruction," *ACM Transactions on Graphics*, vol. 32, no. 3, pp. 29:1–29:13, Jul. 2013.

[32] K. P. Murphy, *Probabilistic Machine Learning: An Introduction*. MIT Press, Mar. 2022.

[33] T. Lewiner, H. Lopes, A. W. Vieira, and G. Tavares, "Efficient Implementation of Marching Cubes' Cases with Topological Guarantees," *Journal of Graphics Tools*, vol. 8, no. 2, pp. 1–15, Jan. 2003.

[34] P. Shilane, P. Min, M. Kazhdan, and T. Funkhouser, "The Princeton Shape Benchmark," in *Proceedings Shape Modeling Applications, 2004*, Jun. 2004, pp. 167–178.

[35] M. Levoy, J. Gerth, B. Curless, and K. Pull, "The stanford 3d scanning repository." [Online]. Available: <https://graphics.stanford.edu/data/3Dscanrep/>

[36] E. Nelson and Z. Ghahramani, "Sparse Gaussian Processes using Pseudo-inputs," in *Advances in Neural Information Processing Systems*, vol. 18. MIT Press, 2005.

[37] M. Titsias, "Variational Learning of Inducing Variables in Sparse Gaussian Processes," in *Proceedings of the Twelfth International Conference on Artificial Intelligence and Statistics*. PMLR, Apr. 2009, pp. 567–574.